Effects of Dark Matter on the Properties of Strange Quark Stars

Jing Huang , Gan Wu , Xiao-Yang Zhang , Jin-Biao Wei , Huan Chen *

Posted Date: 27 February 2026

doi: 10.20944/preprints202602.1818.v1

Keywords: strange quark stars; dark matter; tidal deformability

 doi:10.20944/preprints202602.1818.v1

Article

Effects of Dark Matter on The properties of Strange Quark Stars

Jing Huang, Gan Wu, Xiao-Yang Zhang, Jin-Biao Wei and Huan Chen *

School of Mathematics and Physics, China University of Geosciences, Lumo Road 388, 430074 Wuhan, China
* Correspondence: huanchen@cug.edu.cn

Abstract

We investigate the effects of dark matter on the properties of strange quark stars within the framework of general relativity with two fluids coupled only with gravity. Adopting the color-flavor locked model for strange quark matter and considering both fermionic (free fermion gas) and bosonic (polytropic) equations of state for dark matter, we systematically study the structure and tidal deformability of dark matter admixed strange stars. Our results show that the presence of dark matter significantly modifies the mass-radius relations, with the maximum mass of dark matter admixed strange stars exhibiting a non-monotonic dependence on the dark matter mass fraction χ - a minimum at an intermediate χ. The tidal deformability Λ of dark matter admixed strange stars shows complex behavior depending on both the stellar mass and dark matter fraction, with $\Lambda - \beta$ (the compact parameter) relations deviating from the universal relations observed for pure strange stars or dark stars. Our findings demonstrate that dark matter admixed strange stars with different configurations but identical masses and radii can be distinguished by their tidal deformabilities, providing potential observational signatures for detecting dark matter in compact astrophysical objects. The results are compared with current astrophysical constraints from gravitational wave observations and pulsar measurements.

Keywords: strange quark stars; dark matter; tidal deformability

1. Introduction

As the most compact observable celestial objects, neutron stars(NSs) with their extreme interior environments serve as natural laboratories for studying fundamental interactions and physics beyond the Standard Model[1]. Theoretical investigations of NSs can be traced back almost a century ago[2–6]. Since the first observation of pulsar by [7], much Observational progress have been made. In August 2017, the binary neutron star merger GW170817[8] confirmed gravitational waves as a second, equally powerful window alongside electromagnetic signals, inaugurating the era of multi-messenger astronomy. Currently operational detectors include LIGO, Virgo and KAGRA, and a new generation of ground-based and space-based instruments will soon expand the network[9–11]. Their results have already provided tight constraints on the theoretical models of NSs[12,13], e.g., the tidal deformability of NSs. In addition, traditional optical methods also provide a large number of refined observations to constrain the properties of NSs, e.g., PSR J0740+6620[14,15], PSR J0030+0451[16,17], HESS J1731-347[18], XTE J1814-338[19].

However, up to now, there are still much uncertainties in the internal composition of NSs, which have motivated a wide range of refined models[20]. The concept of strange stars(SS) composed entirely of self-bound strange quark matter(SQM)[21–24], has been studied for nearly half a century. It provides a unique observational window into the properties of matter within the low-temperature, high-density regime of the quantum chromodynamics(QCD) phase diagram. Recent astronomical observations[25–28] provide more and more candidates of SSs, e.g., the widely discussed HESS J1731-347[18].

The equation of state(EOS) of SQM reflects its macroscopic properties and provides a key input for studying the SS structure. Yet, many uncertainties persist due to the difficulty in solving the

 doi:10.20944/preprints202602.1818.v1

nonperturbative QCD. Therefore, various effective models have been proposed, such as MIT bag model[29,30], Color-Flavor Locked(CFL) model[31], Nambu-Jonna-Lasino model[32], quasi-particle model[33], confining density-dependent mass model[34], and models based on the Dyson-Schwinger equations[35–39], etc. They try to reproduce some of the most important properties of QCD, such as asymptotic freedom, confinement, dynamical chiral symmetry breaking and its restoration, as well as the color-superconductivity, and can reach somehow successful descriptions of hybrid NSs or SSs.

On the other hand, dark matter (DM), first hypothesized by Zwicky[40] in the 1920s and steadily corroborated by subsequent observations[41–43], has become one of the most formidable open problems in contemporary physics. Its extremely weak interaction with ordinary matter leaves its intrinsic properties almost entirely unknown. Various conjectures of the particles of DM have been proposed[44], but not yet confirmed by any experiments[45]. Over the past three decades, several groups have advanced the idea that NSs, whose bulk properties are comparatively accessible, can be used as astrophysical laboratories to probe DM[46–49]. As a result, a growing body of work has systematically incorporates the effects of DM on NSs [50–55]. In this work, we focus on DM admixed SSs(DSSs), which also attracts much attention recently[56–65]. They investigate properties of DSSs, e.g., the mass-radius relations, tidal deformability, radial oscillations etc, with various EOSs of SQM and DM, as well as comparisons with astrophysical observations.

In this paper, we aim to investigate the effects of DM on the properties of SSs, adopting various models of EoS for SQM and DM. We will explore how the presence of DM influences the mass-radius relations and tidal deformability of SSs. The paper is organized as follows. In Section 2, we introduce the EOSs for SQM and DM respectively. In Section 3, we introduce the equations of the static structure and the tidal deformability for two-fluid stars. In Section 4, we present our numerical results on the structure and the tidal deformability of the DSSs. At last, we draw a short summary. Throughout the paper, we use natural units where $c = \hbar = 1$, with c and $\hbar$ being the speed of light in vacuum and the reduced Planck constant, respectively.

2. EOS for SQM and DM

The EOS describes the relationship between the pressure P and energy density ϵ of matter, usually written as $P = P(\epsilon)$. It plays a fundamental role in studying the structure and evolution of stars, as different EOSs lead to distinct predictions of their properties. In the study of NSs and SSs, the EOS directly affects the mass, radius, and internal structure of these stars. In the following, we introduce our adopted EOSs for SQM and DM.

2.1. Strange Quark Matter

In the density region of the interior of compact stars, perturbative QCD and first-principle non-perturbative QCD calculations suffer from severe problems. Therefore, phenomenological models are widely used to describe the EOS for SQM. In this work, we use the CFL model to describe SQM.

The CFL model is an improved bag model by considering the color-superconductivity at high densities. The MIT bag model, introduced in Ref. [29,30], describe the quark matter as free particle combined in a bag, with a bag constant B to simulate the quark confinement. Specifically, the bag constant B contributes negatively to the pressure of QM and positively to the energy density. This means the equation of state for QM is shifted relative to that of a free Fermi gas, resulting a lower pressure for QM at the same energy density. Its EOS takes an extremely simple form in zero-temperature and massless case, given explicitly as:

$$p = \frac{1}{3}(\epsilon - 4B). \tag{1}$$

Due to the simplicity, it is often used as a bench mark for studying SQM and SSs.

 doi:10.20944/preprints202602.1818.v1

The CFL model, introduced in Ref. [31], improve the bag model by taking into account the influences of the energy gap Δ of the color superconductivity. The corresponding EOS[66,67] can be expressed as follows:

$$\epsilon(p) = 4B + 3p - \frac{9\alpha\mu^2}{\pi^2} \tag{2}$$

$$\alpha = \frac{2\Delta^2}{3} - \frac{m_s^2}{6}, \tag{3}$$

$$\mu^2 = -3\alpha + \sqrt{9\alpha^2 + \frac{4}{3}\pi^2(B+p)}, \tag{4}$$

where m_s is the mass of the strange quark and Δ is the energy gap of the color superconductivity. The CFL model is thoroughly investigated in [67] concerning the observational constraints of NSs.

2.2. Dark Matter

Due to our ignorance on DM, its EOS remain highly uncertain, various models have been proposed to calculate its EOS. Basically, a possible particle of DM can be one of the two fundamental types: a fermion or a boson. In this work, we will adopt two types of models for the DM EOS accordingly. One is the the free fermion gas EOS, as a representative of the former, and the other is a polytropic EOS [68] as a representative of the latter.

The free fermion gas model was widely used in studying DM admixed NSs or DSSs[50,58,60,62]. For the free fermion gas with a finite DM particle mass (DPM), the pressure and energy density are given as

$$\epsilon_{free} = \frac{m_D^4}{8\pi^2}[(X_F + 2X_F^3)\sqrt{1+X_F^2} - sinh^{-1}(X_F)], \tag{5}$$

$$p_{free} = \frac{m_D^4}{24\pi^2}[(-3X_F + 2X_F^3)\sqrt{1+X_F^2} + 3sinh^{-1}(X_F)], \tag{6}$$

where $X_F = \frac{k_F}{m_D}$, m_D is the mass of the DM particle, and k_F is the Fermi momentum.

For the Boson-type DM, we adopt a widely used EOS based on the Gross Pitaevskii equation, which is a polytropic EOS used to describe the Bose-Einstein condensate stars [68]. The corresponding EOS is expressed as follows:

$$p(\epsilon) = K\epsilon^2 = \frac{2\pi a}{m_D^3}\epsilon^2, \tag{7}$$

where $a = 1$ fm is the scattering length, m_D is the mass of the DM particle.

3. Structure and Tidal Deformability of a Dark Matter Admixed Strange Star

In combination of the above EOSs, one can obtain macroscopic properties of NSs by solving equations from general relativity. In the following, we will show the static structure equations that impose self-gravitating equilibrium on the DSSs. We will also show the equation for the tidal deformability of a DSS, presenting its linear response to an external tidal field during a binary inspiral.

3.1. Structure Equations

The so called TOV equation proposed in 1930s[5,6] gave the first structure equations for a spherically symmetric static NS.

To obtain the properties of compact stars under strong gravitational field, one starts from the Einstein field equation, i.e.,

$$R_{\mu\nu} - \frac{1}{2}Rg_{\mu\nu} = -8\pi G T_{\mu\nu}, \tag{8}$$

 doi:10.20944/preprints202602.1818.v1

where $g_{\mu\nu}$ and $T_{\mu\nu}$ represent the metric tensor and energy momentum tensor respectively, $R_{\mu\nu}$ and R represent the Ricci tensor and Ricci scalar respectively, determined by the metric tensor and its partial derivatives. For the static and spherically symmetric case, the metric takes the form as

$$ds^2 = e^{\nu(r)}dt^2 - e^{\lambda(r)}dr^2 - r^2d\theta^2 - r^2sin\theta^2d\phi^2, \tag{9}$$

where $\nu(r)$ and $\lambda(r)$ represent the metric functions and we take the sign to be (+,-,-,-). The matter in a NS is regarded as a perfect fluid, so its energy momentum tensor can be written as

$$T^{\mu\nu} = (\epsilon + p)u^\mu u^\nu + pg^{\mu\nu}, \tag{10}$$

where $u^\mu = \frac{dx^\mu}{d\tau}$ represent the contra-variant form of a four-velocity. For a static star, the energy momentum tensor could be written as $T^\mu_\nu = diag(\epsilon, -p, -p, -p)$.

Putting the metric tensor and energy momentum tensor into Eq. (8), one can obtain the famous TOV equations:

$$\frac{dp}{dr} = -\frac{G(m + 4\pi r^3 p)}{r^2(1 - 2Gm/r)}(p + \epsilon), \tag{11}$$

$$\frac{dm}{dr} = 4\pi r^2 \epsilon, \tag{12}$$

With a central pressure p_c and integrating from $r = 0$ until $p(r = R) = 0$, one can obtain the mass $M = m(R)$ and radius R of a Ns. The metric functions can be obtained by

$$e^{-\lambda} = 1 - \frac{2Gm}{r}, \tag{13}$$

$$\frac{d\nu}{dr} = \frac{2G(m + 4\pi r^3 p)}{r^2(1 - 2Gm/r)}, \tag{14}$$

with a boundary condition $\nu(r = \infty) = 0$.

For a two-fluid system coupled only through gravity, its energy moment tensor can be written as a summation of the two individual fluids $T^{\mu\nu} = \sum_i T_i^{\mu\nu}$ with the subscript i representing SQM or DM. Each fluid obeys the energy-moment conservation, i.e., $\nabla_\mu T_i^{\mu\nu} = 0$. The corresponding static structure equations for a DSS can be obtained as the following form [69]

$$\frac{dp_i}{dr} = -\frac{G(m_{tot} + 4\pi r^3 p_{tot})}{r^2(1 - 2Gm_{tot}/r)}(p_i + \epsilon_i), \tag{15}$$

$$\frac{dm_i}{dr} = 4\pi r^2 \epsilon_i, \tag{16}$$

where $m_{tot} = \sum_i m_i$ and $p_{tot} = \sum_i p_i$. Starting with central pressures $p_{c,q}$ and $p_{c,d}$ for SQM and DM respectively, and integrating from $r = 0$ until both $p_q(r = R_q) = 0$ and $p_d(r = R_d) = 0$, one obtains the structure of a DSS. NB, there are two different radius R_q and R_d for SQM and DM respectively. Usually we take the larger one as the radius R of a DSS, while the radius R_q is also called the visible radius. When $R_q < R_d$, the stellar outer layer composed of DM is called the dark halo. The mass of a DSS is the total mass $M = m_{tot}(R)$. The corresponding metric functions are given by

$$e^{-\lambda} = 1 - \frac{2Gm_{tot}}{r}, \tag{17}$$

$$\frac{d\nu}{dr} = \frac{2G(m_{tot} + 4\pi r^3 p_{tot})}{r^2(1 - 2Gm_{tot}/r)}, \tag{18}$$

with the boundary condition $\nu(r = \infty) = 0$.

 doi:10.20944/preprints202602.1818.v1

3.2. Tidal Deformability

Tidal deformability is also an important property of NS, which can be measured through the gravitational wave radiation from binary-NS inspiral. The tidal deformability Λ can be obtained by

$$\Lambda = \frac{2}{3} k_2 \beta^{-5}, \tag{19}$$

where $\beta = \frac{GM}{R}$ represents the compactness of a star and k_2 is the $l = 2$ tidal Love number, which can be expressed as:

$$\begin{aligned} k_2 = {} & \frac{5}{8}(1-\beta)^2\beta^5[2C(y_R - 1 - y_R + 2)] \\ & \times \{2\beta[(4y_R+1)\beta^4 + (6y_R-4)\beta^3 + (26-22y_R)\beta^2 + 3(5y_R-8)\beta - 3y_R + 6] \\ & + 3(1-2\beta)^2[2\beta(y_R-1) - y_R + 2] ln(1-2\beta)\}^{-1}, \end{aligned} \tag{20}$$

where the variable $y_R \equiv y(R) = [rH'(r)/H(r)]_{r=R}$ is the logarithmic derivative for metric perturbation $H(r)$ [70,71]. The function $y(r)$ satisfies the differential equation [72,73]

$$r\frac{dy(r)}{dr} + y^2(r) + y(r)F(r) + r^2Q(r) = 0, \tag{21}$$

with

$$F(r) = \frac{r - 4\pi G r^3 \sum_i (\epsilon_i - p_i)}{r - 2GM}, \tag{22}$$

$$\begin{aligned} Q(r) = {} & \frac{4\pi G r}{r-2GM} \times \{\sum_i [5\epsilon_i + 9p_i + \frac{\partial \epsilon_i}{\partial p_i}(\epsilon_i + p_i)] - \frac{6}{4\pi G r^2}\} \\ & - [\frac{8\pi G r^3 \sum_i p_i + 2GM}{r(r-2GM)}]^2. \end{aligned} \tag{23}$$

Eq. (21) depends on the internal distributions of pressure and energy density in a DSS and can be solved simultaneously with the structure equations Eq. (15) and Eq. (16). In addition, the boundary condition of $y(r=0) = 2$ is indispensable, where the detailed derivation can be found in reference [70]. Furthermore, the energy density of SQM does not decrease to 0 at its surface, i.e., it behaves as a step function. Consequently, the term $\frac{\partial \epsilon_i}{\partial p_i}$ in $Q(r)$ behaves as a δ function, which gives an extra contribution to the integration of $y(r)$. Therefore, one need to give a modification of $y(r)$ at the SQM surface R_q [71,74]

$$y(R_q^+) - y(R_q^-) = -\frac{4\pi R_q^3 \Delta\epsilon}{m_{tot}(R_q) + 4\pi R_q^3 p_{tot}(R_q)}. \tag{24}$$

where $\Delta\epsilon = \epsilon(R_q^+) - \epsilon(R_q^-)$ represents the gap of energy density.

4. Results and Discussion

In this section, we show our results for EOSs of SQM and DM, properties of pure SSs and DM stars (DSs), as well as properties of DSS.

4.1. Properties of Pure Strange Stars and Dark Matter Stars

Employing the analytical expressions Eq. (1), (2), (7), we can obtain the various EoSs of SQM and DM. Our numerical results of the various EOSs are shown in Figure 1. For the CFL model of SQM, there are three main parameters, the bag constant B, the energy gap of color superconductivity Δ and the strange quark mass m_s. They are thoroughly investigated in Ref.[67] to fit present astrophysical observations. Herein, we take the parameter set $B = 70$ MeVfm^{-3}, $\Delta = 160$ MeV, $m_s = 150$ MeV,

 doi:10.20944/preprints202602.1818.v1

which can best fit NS observation data shown in Figure 1. For comparison, we also show the result of MIT bag model with bag constant $B = 60$ MeVfm^{-3} and $B = 90$ MeVfm^{-3}, abbreviated as CFL, MIT60, MIT90 respectively. One can see that the EOS with the CFL model are stiffer than the MIT bag model. Note that there are always a lower bound of the energy density for SQM, due to quark confinement characterized by the bag constant. For DM, we employ the free fermionic EOSs and polytropic bosonic EOSs. Now the only parameter in the DM models is the DPM. Since only when the DPM is close to the typical mass scale $1GeV$ in SSs that it can strongly influence the structure of SSs, we take $m_D = 0.5$ GeV, 1 GeV, 2 GeV representing three typical cases. In the following, the free fermionic EOSs and polytropic bosonic EOSs are abbreviated as FF and PB respectively, with the following number representing the corresponding DPM. We can see that for each model of DM, the EOS is stiffer with decreasing of the DPM. In comparison with the free fermionic DM, the polytropic EOSs of Bosonic DM are softer at low densities but become stiffer at large densities. The properties of EOSs determine the properties of corresponding stellar structures, and the corresponding central pressure of the pure SSs and DSs with the maximum masses are also marked in Figure 2.

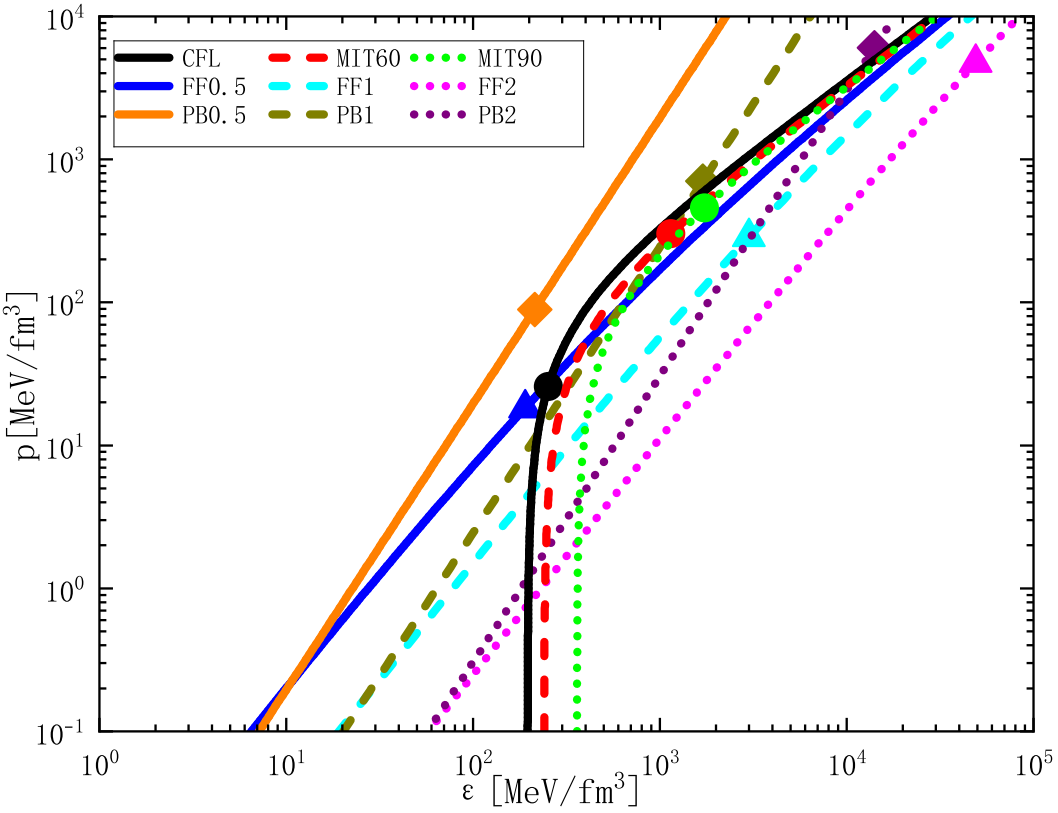

Figure 1. The pressure as a function of energy density for SQM and DM. The different line types/colors indicate different models/parameters: CFL quark model(CFL, solid black), MIT bag model with $B = 60$ MeVfm^{-3}(MIT60, dashed red), or $B = 90$ MeVfm^{-3}(MIT90, dotted green); free fermionic DM with $m_D = 0.5$ GeV(FF0.5, solid blue), $m_D = 1$ GeV(FF1, dashed cyan), and $m_D = 2$ GeV(FF2, dotted magenta); polytropic bosonic DM with $m_D = 0.5$ GeV(PB0.5, solid orange), $m_D = 1$ GeV(PB1, dashed olive), and $m_D = 2$ GeV(PB2, dotted purple). The p_c and ϵ_c of pure SSs and DSs with their maximum masses are also marked.

 doi:10.20944/preprints202602.1818.v1

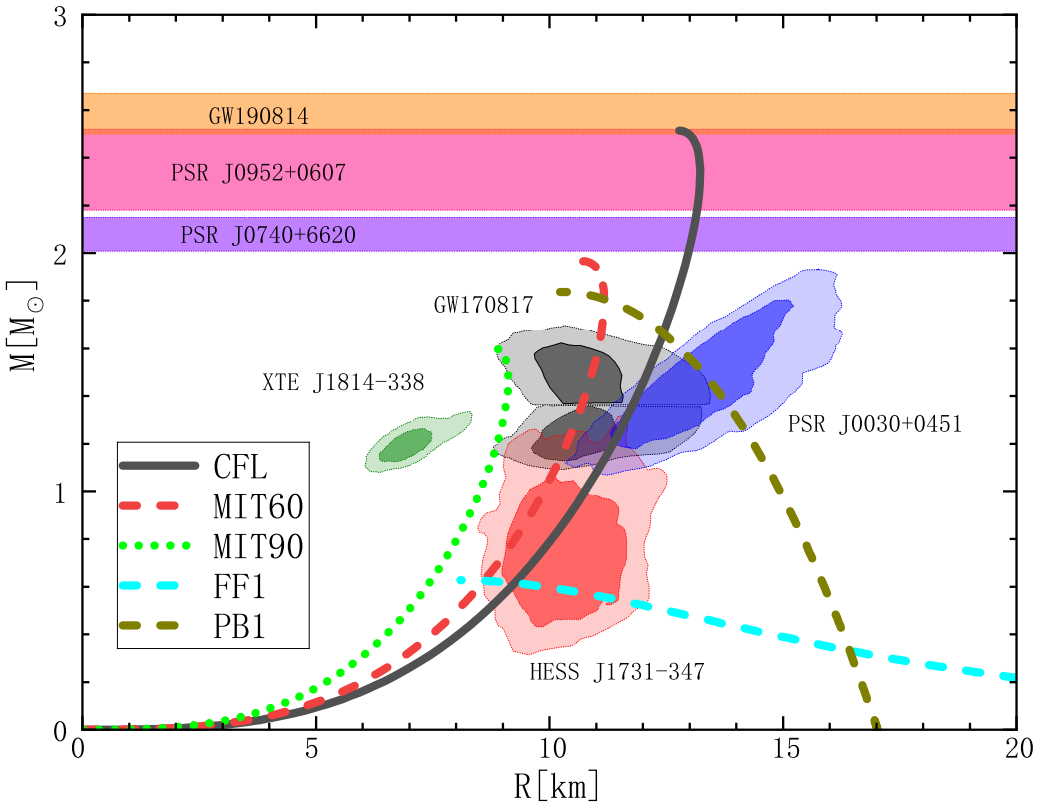

Figure 2. The mass as a function of radius for pure SSs and DSs with various EOSs. The correspondence between line types/colors and EOSs are the same as in Figure 1. Some results of DSs are not shown due to their too large/small mass/radius. The colored regions represent a selection of recent pulsar observational constrains, see the text for details.

Combing with the above EOSs, we solve the TOV equations and obtain Mass-Radius relations of pure SSs and DSs. The results of SSs are show in Figure 2. Meanwhile, we also show a selection of recent pulsar observational constrains in Figure 2, including GW170817[12], HESS[18], PSR J0030+0451[16,17], XTE J1814-338[19], GW190814[75], PSR J0952+0607[76], PSR J0740+6620[14,15]. In comparison with the MIT bag model, SQM with the CFL model can support SSs with $M_{max} > 2.5M_{\odot}$, consistent with present observational constraints on pulsar maximum mass. With our employed parameter, it can best fit nearly all the pulsar observational data in the figure, except the one of XTE J1814-338. Note that the data of XTE J1814-338 can not be explained by SSs by resetting the parameters in CFL model or MIT bag model. We also show results of DSs with FF1 and PB1 in Figure 2. With such models and parameters, the DSs have similar radius but decrease with increasing stellar masses, which is a little smaller than SSs. The maximum mass and typical radius of DSs are sensitive to the DPMes. They decrease quickly with increasing of the DPMes. The maximum masses and the corresponding radii, central densities of pure SSs and DSs with various EOSs and parameters are shown in Table 1. The maximum mass of pure DSs with polytropic bosonic EOS is larger than that with the free fermionic EOS and the same DPM.

In Figure 3, we show the tidal deformability of pure SSs and DSs, depending on the stellar mass (left panel) and the compact parameter (right panel),respectively. The constraint from GW170817 is also shown in the figure. In all the cases, the tidal deformability decrease with increasing stellar mass. The minimum values of the tidal deformability are similar for SSs with different models, and their dependence on the compact parameter is almost universal. For SSs with CFL model, the corresponding tidal deformability with $M = 1.4M_{\odot}$ is a little higher than the observational constraint or the results with the MIT bag model. For pure DSs the minimum values of tidal deformability depend strongly on the DM model but quite insensitive to the the DPMes. For pure DSs with free fermionic EOSs, the tidal deformability are all above 1 thousand. while the minimum values with polytropic bosonic EOSs

 doi:10.20944/preprints202602.1818.v1

can reach below 1 hundred, similar as SSs. For DSs, the dependence of the tidal deformability on the compact parameter deviates from the universal relation of SSs, and depends on the various models, but not on DPMes.

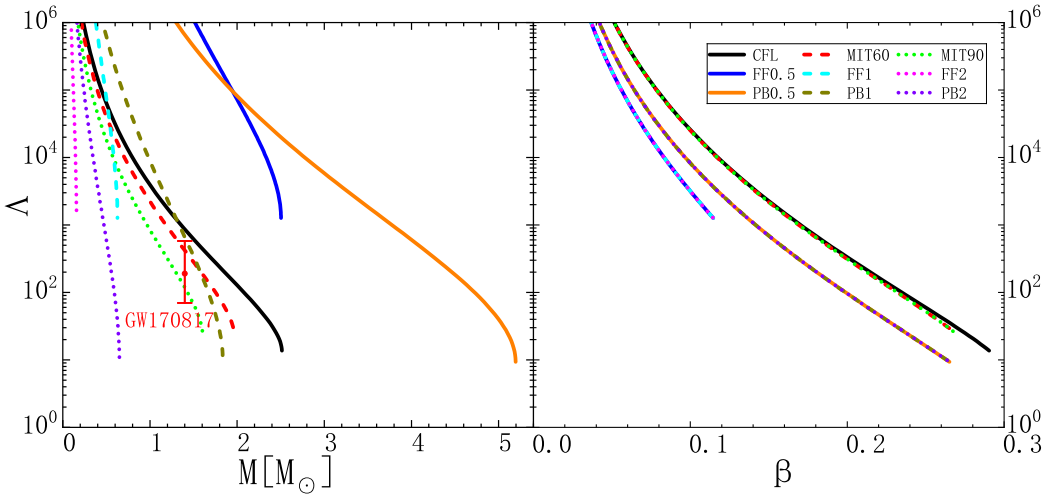

Figure 3. The tidal deformability Λ as a function of mass M (left panel) and compactness β (right panel) for pure SSs and DSs with various EOSs. The correspondence between line types/colors and EOSs are the same as in Figure 1. The observational constraint from GW170817 is indicated by a red error bar.

Table 1. Some typical properties of pure SSs and DSs with various EOSs and parameters.

Model	$M_{max}(M_\odot)$	$R_{M_{max}}$(km)	$\epsilon_{c,M_{max}}$(MeVfm^{-3})	$\Lambda_{1.4}$
CFL	2.51	12.77	808	862
MIT60	1.97	10.72	1146	417
MIT90	1.60	8.75	1731	118
FF0.5	2.50	32.28	190	1,948,900
FF1	0.63	8.11	2994	-
FF2	0.16	2.01	49160	-
PB0.5	5.20	28.98	214	658,065
PB1	1.84	10.27	1698	660
PB2	0.65	3.60	14060	-

4.2. Properties of Dark Matter Admixed Strange Stars

In combination with the above EOSs of SQM and DM, we solve the equations for two-fluid stars, obtaining the structure and tidal deformability of DSSs.

As discussed above, there are two independent central pressures for SQM and DM respectively to determine the configuration of a two-fluid star. Therefore, the mass-radius relations can not be given by a single curve as for single-fluid stars. In Figure 4, we show the masses of DSSs depending on the radius (left panels) and the SQM radius (right panels) with fixed DM fraction $\chi = \frac{M_d}{M}$. We choose $\chi = 0, 0.1, 0.3, 0.5, 0.7, 0.9, 1$ as presentative. From top to bottom panels, we take DPM $m_D = 0.5, 1, 2$ GeV respectively. Several works in the literature [61,62,77] on the radial oscillations of two-fluid stars show that the maximum mass with fixed χ are coincident with the critical points of stability. Therefore, we truncate the curves at the maximum masses for fixed χ. In Figure 4, one can see that with a small fraction of DM, e.g., $\chi = 0.1$, the maximum mass of DSSs decreases a little from that of pure SSs. Meanwhile, the radius of a DSS, given by the radius of SQM, is also a little smaller than the SS with the same mass. As the stellar mass decreasing, the radius of DSS changes like the SSs until the radius of SQM equals the radius of DM. Then, the radius of DSS, given by the radius of DM, increases as the stellar mass further decreases, even intersecting with curves corresponding to smaller χ. In contrast, the raduis of SQM always looks like that of SSs and decreases with χ increasing, as shown in the right panels. As the DM fraction increases, the maximum mass of DSS decreases and then increases until $\chi = 1$. With a large χ, the DM radius can be larger than the SQM radius even at the maximum mass

 doi:10.20944/preprints202602.1818.v1

and it always increases as stellar mass decreases. Comparing the results with different DPM, one can see qualitatively similar effects of DM on the stellar maximum masses and M-R curves. Quantitatively, with larger DPM, the DM radius become dominant with smaller stellar masses or larger DM fractions. concerning the the data of XTE J1814-338, we note that the visible SQM radius always decreases with χ and can reach that of XTE J1814-338. Therefore, when DPM is not too large that the maximum mass of DSSs decreases too fast with χ, the DSSs would cover the data of XTE J1814-338.

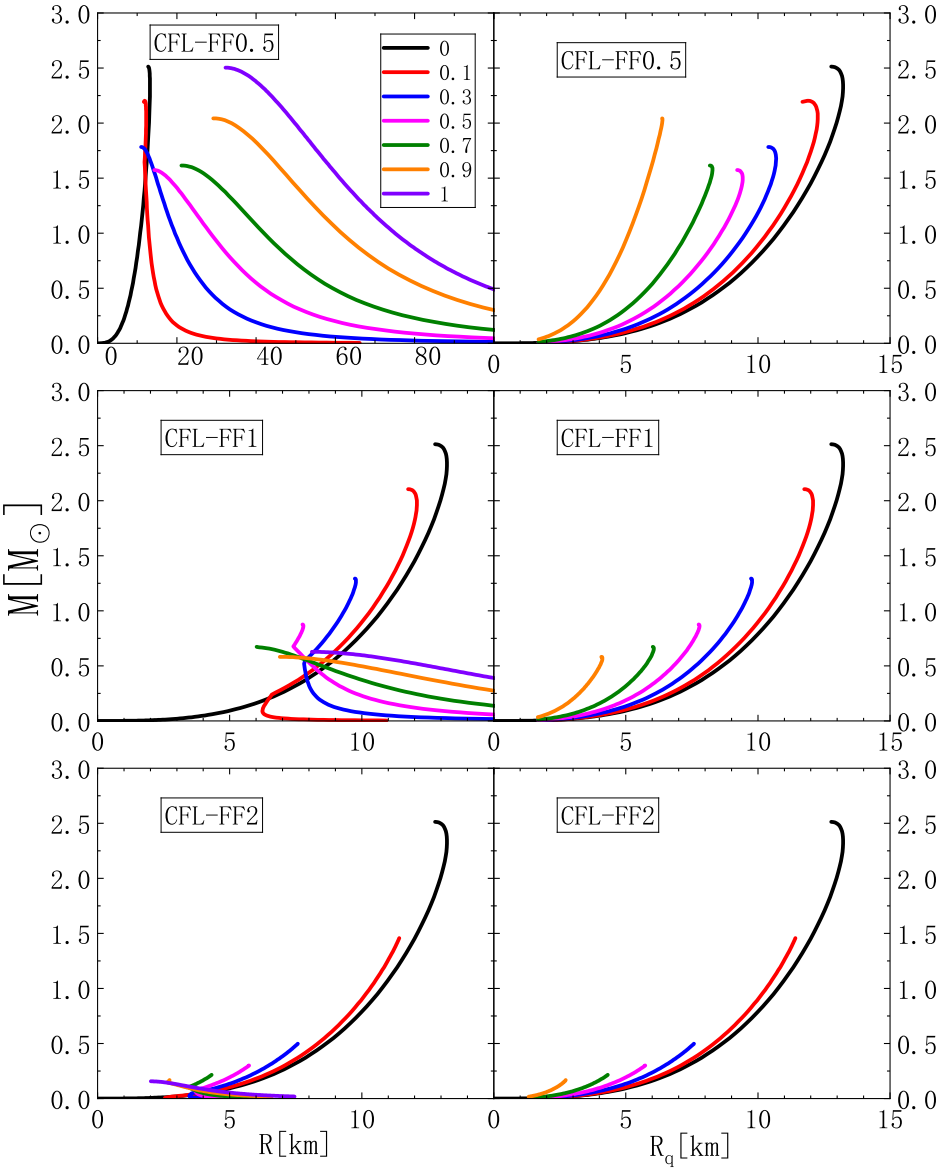

Figure 4. The mass as a function of radius (left panels) or SQM radius (right panels) for DSSs withc. From top to bottom panels, $m_D = 0.5$ GeV (CFL-FF0.5), 1 GeV (CFL-FF1), and 2 GeV (CFL-FF2), respectively. Different line colors represent different DM fractions: black ($\chi = 0$), red ($\chi = 0.1$), blue ($\chi = 0.3$), green ($\chi = 0.5$), magenta ($\chi = 0.7$), orange ($\chi = 0.9$), and purple ($\chi = 1$).

In Figure 5, we show the mass of DSSs depending on the radius (left panels) and the SQM radius (right panels) with polytropic bosonic EOS. Again, one can find similar qualitative properties of DSSs as in Figure 4. Quantitatively, the M-R relations of DSSs are quite dependent on the structure of pure DSs. Since the maximum mass and radius of DSs with polytropic bosonic EOS are larger than that with free fermionic EOS and the same DPM, the M-R relations of DSSs with polytropic bosonic EOS are similar as that with free fermionic EOS but a smaller DPM.

 doi:10.20944/preprints202602.1818.v1

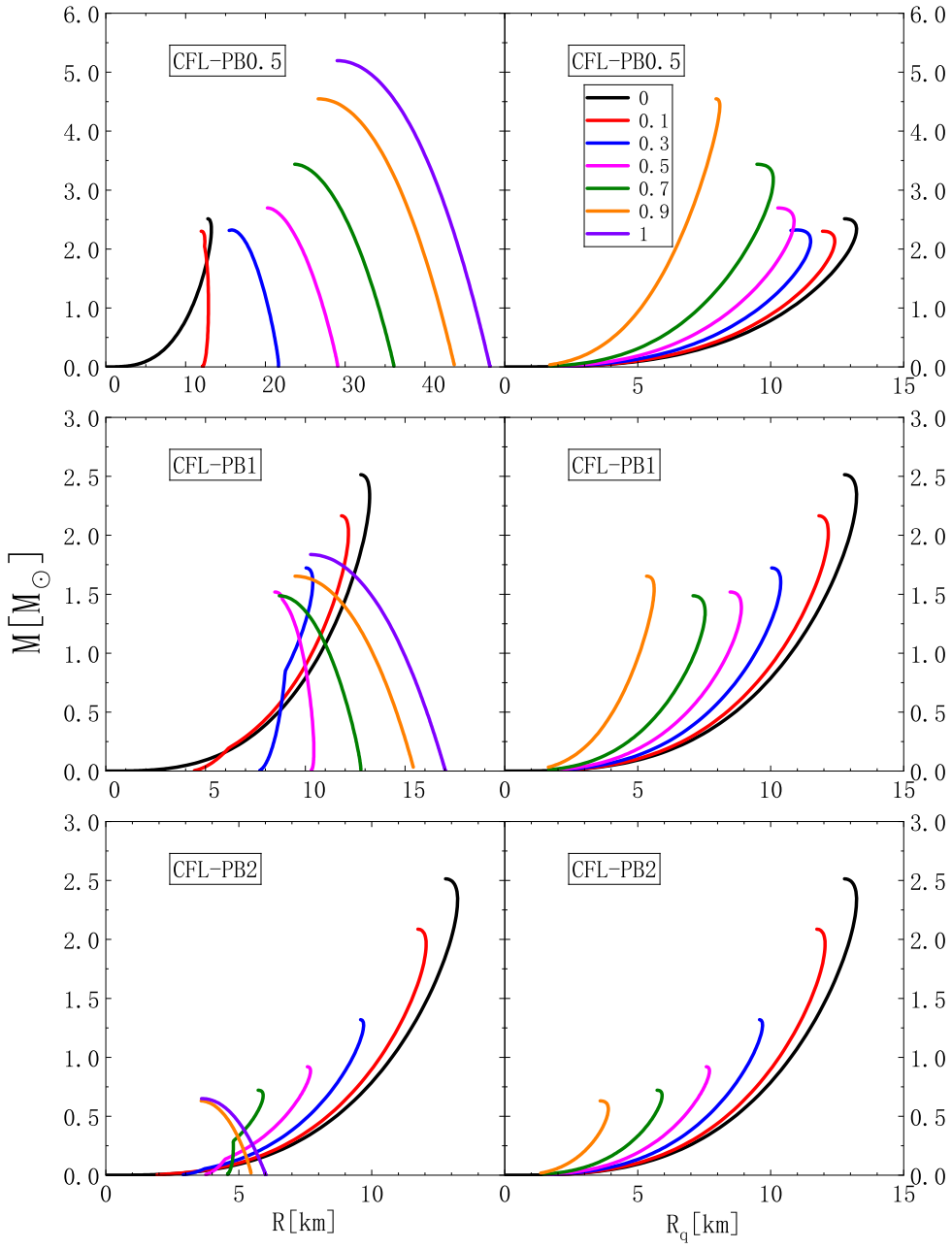

Figure 5. The mass as a function of radius (left panels) and SQM radius (right panels) for DSSs with polytropic bosonic EOS of DM. From top to bottom panels, $m_D = 0.5$ GeV, 1 GeV, and 2 GeV, respectively. Different line colors represent the same as in Figure 4.

To see more clearly the change of the maximum mass of DSSs with different χ, we show the variation of the maximum mass with χ in Figure 6. Qualitatively, there is a common feature in all the cases: the maximum mass decreases from $\chi = 0$ to a minimum and then increases until $\chi = 1$. Quantitatively, the position of the minimum of the curves depends strongly on the maximum mass of DSs. When the maximum masses of DSs and SSs are similar, the minimum appear close to $\chi = 0.5$. However, when the maximum masses of DSs and SSs are quite different, the minimum values appear quite close to the lower end. For example, in cases of CFL-FF2 and CFL-PB0.5, the minimum values lie at $\chi = 0.99$ and $\chi = 0.17$ respectively.

 doi:10.20944/preprints202602.1818.v1

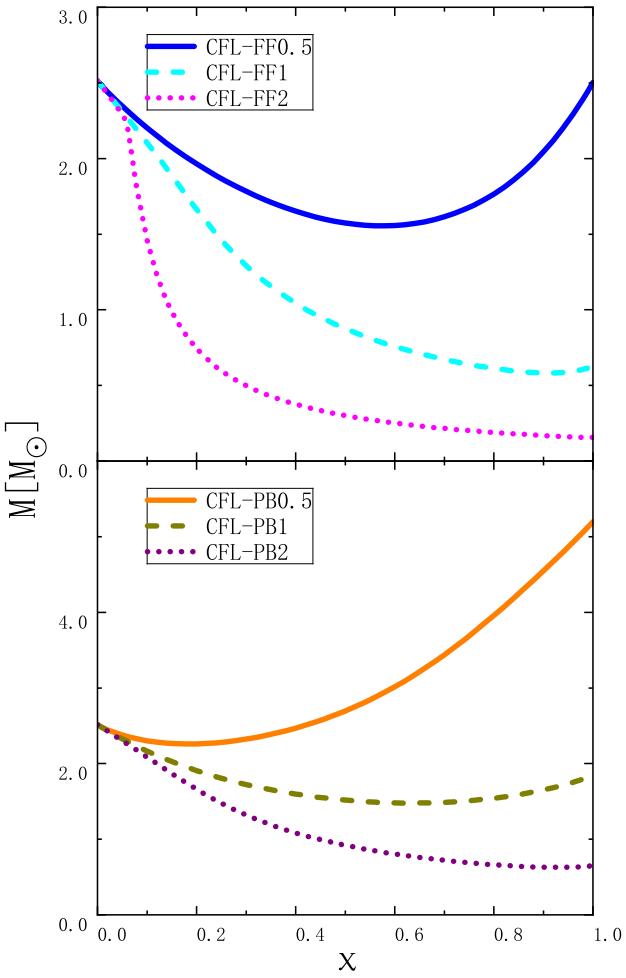

Figure 6. The maximum mass as a function of DM fraction for DSSs with with polytropic bosonic EOS of DM (upper panel) or polytropic bosonic EOS of DM (lower panel). The correspondence between line types/colors and EOS of DM are the same as in Figure 1.

Concerning the stability of DSS, strictly speaking, it is given by the positivity of the square of the lowest radial oscillations frequency. However, there are also some other commonly used criteria for one-fluid stars, one of which is expressed as $\frac{dM}{d\epsilon_c} \geq 0$. In Figure 7, we present the dependence of the DSS masses on the total central energy density ϵ_c, along fixed χ. One can see that with fixed χ, $\frac{dM}{d\epsilon_c} \geq 0$ until the maximum masses, which is consistent with the criteria from radial oscillations.

In Figure 8, we show the contour plot of DSS mass as a function of central pressures of SQM and DM, with fermionic EOS (left panels) or polytropic bosonic EOS (right panels) and $m_D = 0.5, 1, 2$ GeV from top to bottom panels, respectively. The color gradient indicates regions corresponding to different DSS masses, with several thin white curves as representative isomass contours. The curves with gradient colors show the representative curves with $\chi = 0.1, 0.2, ..., 0.9$, ended at corresponding maximum masses. The black curves, determined by the maximum-mass points with various DM fractions, thus show the boundary of the stable stellar configurations. Obviously, when fixing one central pressure and varying the other central pressure, the point with the maximum mass would not be coincident with the critical stable point. Furthermore, in the center of DSSs, the pressures of SQM and DM can be much larger than the maximum central pressures of pure SSs or DSs, e.g., in the left top and left bottom panels. It might have impacts on the cooling of the stars.

 doi:10.20944/preprints202602.1818.v1

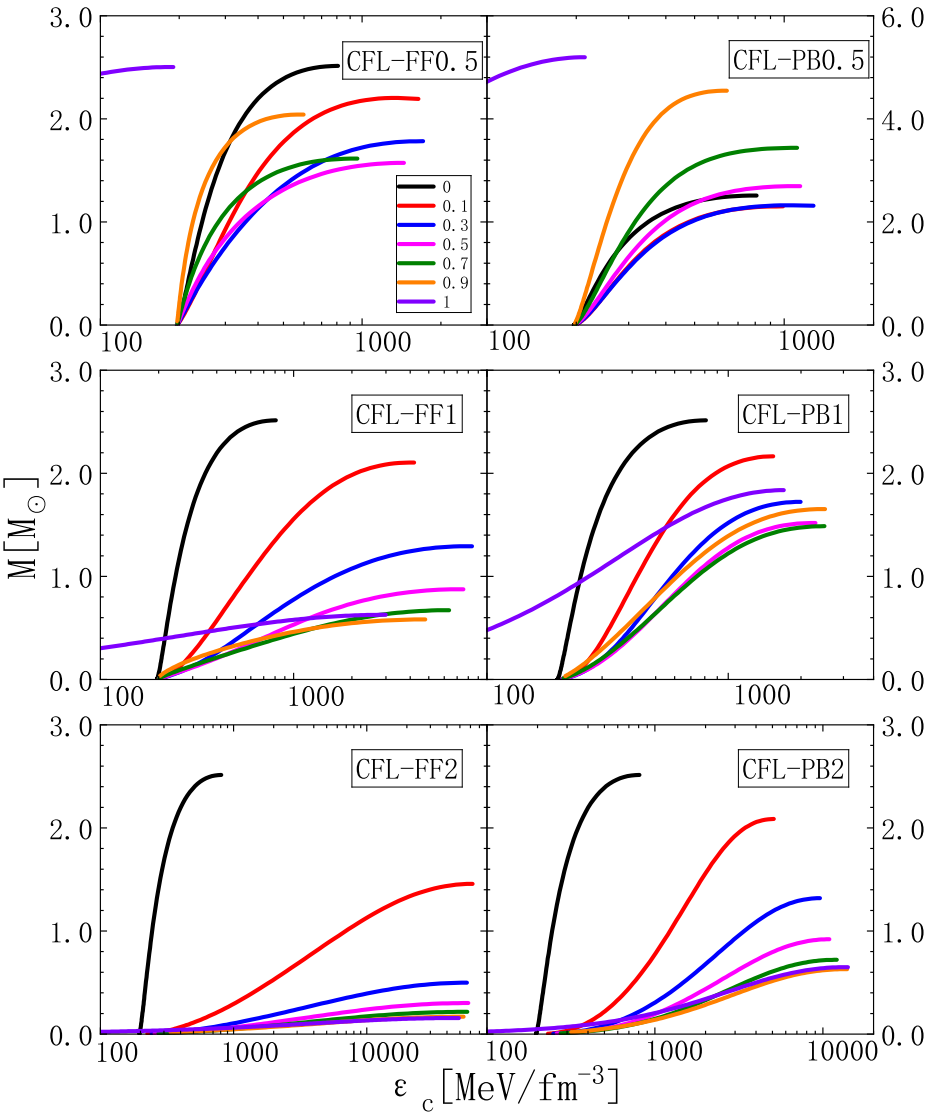

Figure 7. The mass as a function of the central energy density ϵ_c for DSSs. From top to bottom panels, $m_D =$ 0.5 GeV, 1 GeV, and 2 GeV, respectively. Different line colors represent the same as in Figure4.

In Figure 9, we present the tidal deformability Λ of DSSs depending on the stellar mass (left panels) and the compact parameter(right panels). We take the free fermionic EOS of DM and $m_D = 0.5, 1, 2$ GeV from top to bottom panels. Similar as one-fluid stars, Λ of DSSs with a fixed χ decreases monotonically as a function of mass, ending with a minimum at the maximum mass. For DSSs with small DM fractions, the minimum value of Λ increases with χ, but still lower than that with the same stellar mass but smaller χ. With the mass decreasing, Λ of DSS increases quickly and at low masses it turns to increase with χ. In contrast, for DSSs with large χ, Λ of DSS with the same masses increases with χ in all the mass regions. These variations of Λ are qualitatively similar as the variations of radius of DSS dependent on χ. However, there are still quantitative difference. One can see that the intersection points of the $\Lambda - M$ curves are different from the intersection points of the $M - R$ curves. Therefore, the different configurations of DSSs with the same stellar mass and radius can be distinguished by their different Λ. Comparing the three panels with different DPM, one can see that as the DPM increases, DSSs with large χ can only reach small maximum mass, and large values of Λ can only reach in low mass region. For example, when $m_D = 1, 2$ GeV only DSSs with low χ can reach 1.4 $M_\odot$ and the corresponding Λ is smaller than that of pure SSs. For the $\Lambda - \beta$ relations of DSSs shown in the right panels, one can see that the curves of DSSs deviate from both the universal relations of SSs and DSs.

 doi:10.20944/preprints202602.1818.v1

Quantitatively, all the curves of DSSs are lower than the SS curve, and some even lower than the pure DSs curve, especially with a low DPM.

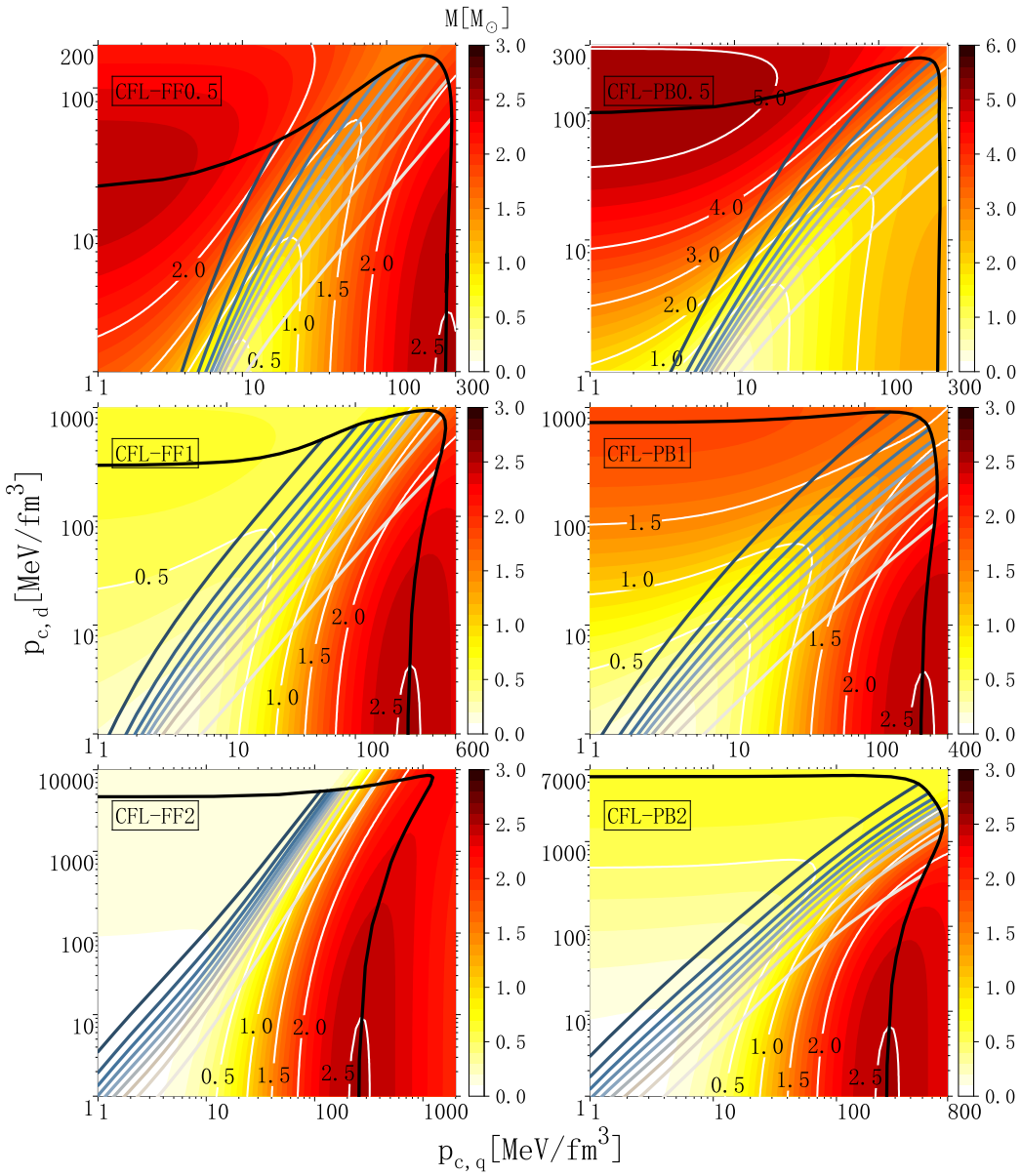

Figure 8. Contour plot of DSS mass as a function of SQM and DM central pressures. The thin white lines correspond to representative isomass contours. The solid curves, colored from light gray to dark blue, correspond to constant-χ curves with χ =0.1, 0.2, . . ., 0.9. The solid black line represents the stability boundary with the maximum mass along fixed χ lines.

 doi:10.20944/preprints202602.1818.v1

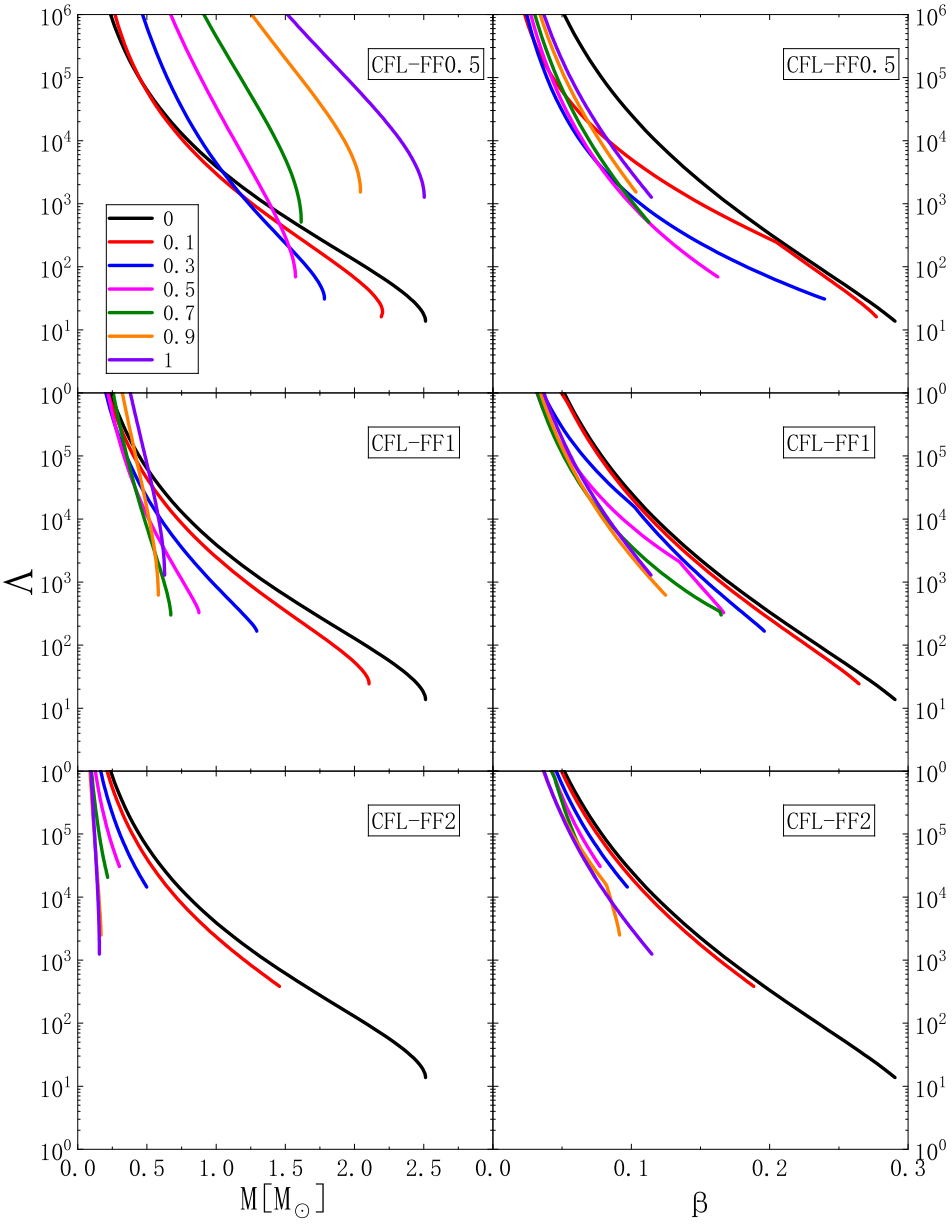

Figure 9. The tidal deformability Λ as a function of mass M (left panel) or compactness β (right panel) for DSSs with free fermionic EOS of DM. From top to bottom panels, $m_D = 0.5$ GeV, 1 GeV, and 2 GeV, respectively. Different line colors represent the same as in Figure4.

In Figure 10 we present the tidal deformability of DSSs with the polytropic bosonic EOS for DM, depending on the stellar mass (left panels) and the compact parameter(right panels), and from top to bottom panels $m_D = 0.5,\ 1,\ 2GeV$ respectively. Qualitatively, the results are similar as those with the free fermionic EOS but smaller DPM. Quantitatively, the variation of the minimum Λ of DSSs with χ is smaller, since the minimum Λ of pure DSs is similar as the SS, while the minimum Λ of pure DSs with the free fermionic EOS is much larger.

 doi:10.20944/preprints202602.1818.v1

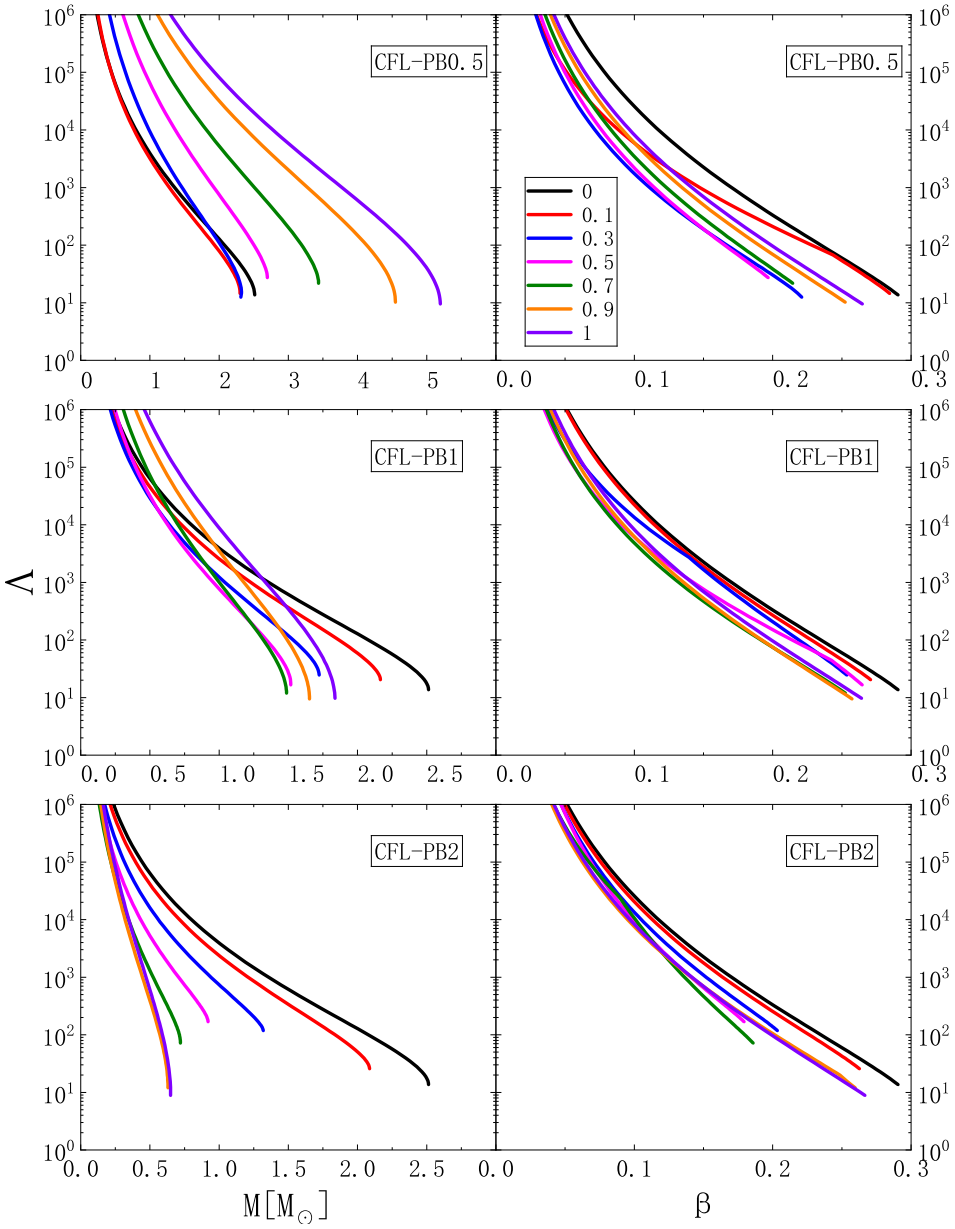

Figure 10. The tidal deformability Λ as a function of mass M (left panel) or compactness β (right panel) for DSSs with polytropic bosonic EOS of DM. From top to bottom panels, $m_D = 0.5$ GeV, 1 GeV, and 2 GeV, respectively. Different line colors represent the same as in Figure4.

5. Summary

In this work, we comprehensively study the DSSs, exploring how DM influences the structural properties and tidal deformability of these compact astrophysical objects. We employ a two-fluid formalism to describe the coupled system of SQM and DM, solving the two-fluid TOV equations for static, spherically symmetric configurations. For the EOSs, We adopt the CFL model of SQM, and two types of models for DM, the free fermion gas model and the polytropic boson model. We compare quantitatively the different influences of the two models, as well as the impacts of the DPM, the key parameter in the DM models.

Our analysis reveals several key findings: (1) The mass-radius relations of DSSs exhibit complex behavior depending on the DM fraction χ, with the maximum mass showing a characteristic minimum at intermediate χ values. (2) The presence of DM generally reduces the (visible) SQM radius compared to pure SSs of the same mass. However, the DM radius can be larger with large DM fractions or with small DM fractions but small stellar masses, forming DM halo. (3) The tidal deformability Λ of DSSs

 doi:10.20944/preprints202602.1818.v1

displays distinctive patterns that deviate from both pure SSs and pure DSs, with the $\Lambda - M$ and $\Lambda - \beta$ relations providing a potential observational discriminant for DM content. (4) The specific behavior depends sensitively on the DM equation of state and particle mass, with fermionic and bosonic DM models yielding quantitatively different predictions.

These results have important implications for multi-messenger astronomy, suggesting that precise measurements of neutron star masses, radii, and tidal deformabilities from gravitational wave observations and electromagnetic observations could potentially constrain the properties of DM. The non-trivial dependence of stellar properties on DM content provides a new avenue for probing DM through astrophysical observations of compact objects. Future observations with next-generation gravitational wave detectors and X-ray timing missions will further test these predictions and potentially reveal signatures of DM in compact stars.

Author Contributions: J. Huang was the main calculator and drafter of the manuscript. X.-Y. Zhang and G.Wu participated in the discussion and part of the data verification. J.-B. Wei guided the main program calculation, and participated in the discussion and revision of the manuscript. H. Chen was the organizer of the project, responsible for organizing the research, the discussion and the revision of the manuscript. All authors have read and agree to the published version of the manuscript.

Funding: We acknowledge financial support from the National Natural Science Foundation of China (Grant Nos. 12205260)

Data Availability Statement: The data presented in this study are available on request from the corresponding author due to college regulations.

Acknowledgments: We thank Prof. Hans-Josef Schulze for helpful discussions.

References

1. Shapiro, S.L.; Teukolsky, S.A., Star Deaths and the Formation of Compact Objects. In *Black Holes, White Dwarfs, and Neutron Stars*; John Wiley and Sons, Ltd, 1983; chapter 1, pp. 1–16.
2. Chadwick, J. Possible existence of a neutron. *Nature* **1932**, *129*, 312–312.
3. Landau, L.D. On the theory of stars. *Phys. Z. Sowjetunion* **1932**, *1*, 285–288.
4. Baade, W.; Zwicky, F. Remarks on super-novae and cosmic rays. *Physical Review* **1934**, *46*, 76.
5. Tolman, R.C. Effect of inhomogeneity on cosmological models. *Proceedings of the National Academy of Sciences* **1934**, *20*, 169–176.
6. Oppenheimer, J.R.; Volkoff, G.M. On massive neutron cores. *Physical Review* **1939**, *55*, 374.
7. Hewish, A.; Bell, S.J.; Pilkington, J.D.H.; Scott, P.F.; Collins, R.A. Observation of a Rapidly Pulsating Radio Source. *Nature* **1968**, *217*, 709–713.
8. Abbott, B.P.; Abbott, R.; Abbott, T.D.; Acernese, F.; Ackley, K.; Adams, C.; Adams, T.; Addesso, P.; Adhikari, R.X.; Adya, V.B.; et al. GW170817: observation of gravitational waves from a binary neutron star inspiral. *Physical Review Letters* **2017**, *119*, 161101.
9. Acernese, F.; Agathos, M.; Agatsuma, K.; Aisa, D.; Allemandou, N.; Allocca, A.; Amarni, J.; Astone, P.; Balestri, G.; Ballardin, G.; et al. Advanced Virgo: a second-generation interferometric gravitational wave detector. *Classical and Quantum Gravity* **2014**, *32*, 024001.
10. Abbott, B.P.; Abbott, R.; Abbott, T.; Abraham, S.; Acernese, F.; Ackley, K.; Adams, C.; Adya, V.; Affeldt, C.; Agathos, M.; et al. Prospects for observing and localizing gravitational-wave transients with Advanced LIGO, Advanced Virgo and KAGRA. *Living reviews in relativity* **2020**, *23*, 3.
11. Bailes, M.; Berger, B.K.; Brady, P.R.; Branchesi, M.; Danzmann, K.; Evans, M.; Holley-Bockelmann, K.; Iyer, B.; Kajita, T.; Katsanevas, S.; et al. Gravitational-wave physics and astronomy in the 2020s and 2030s. *Nature Reviews Physics* **2021**, *3*, 344–366.
12. Abbott, B.P.; Abbott, R.; Abbott, T.; Acernese, F.; Ackley, K.; Adams, C.; Adams, T.; Addesso, P.; Adhikari, R.X.; Adya, V.B.; et al. GW170817: Measurements of neutron star radii and equation of state. *Physical Review Letters* **2018**, *121*, 161101.
13. Abbott, B.P.; Abbott, R.; Abbott, T.; Abraham, S.; Acernese, F.; Ackley, K.; Adams, C.; Adhikari, R.; Adya, V.; Affeldt, C.; et al. GW190425: Observation of a compact binary coalescence with total mass 3.4 $M_\odot$. *The Astrophysical Journal* **2020**, *892*, L3.

 doi:10.20944/preprints202602.1818.v1

14. Miller, M.; Lamb, F.K.; Dittmann, A.; Bogdanov, S.; Arzoumanian, Z.; Gendreau, K.C.; Guillot, S.; Harding, A.; Ho, W.; Lattimer, J.; et al. PSR J0030+ 0451 mass and radius from NICER data and implications for the properties of neutron star matter. *The Astrophysical Journal Letters* **2019**, *887*, L24.
15. Riley, T.E.; Watts, A.L.; Bogdanov, S.; Ray, P.S.; Ludlam, R.M.; Guillot, S.; Arzoumanian, Z.; Baker, C.L.; Bilous, A.V.; Chakrabarty, D.; et al. A NICER view of PSR J0030+ 0451: millisecond pulsar parameter estimation. *The Astrophysical Journal Letters* **2019**, *887*, L21.
16. Miller, M.C.; Lamb, F.; Dittmann, A.; Bogdanov, S.; Arzoumanian, Z.; Gendreau, K.; Guillot, S.; Ho, W.; Lattimer, J.; Loewenstein, M.; et al. The radius of PSR J0740+ 6620 from NICER and XMM-Newton data. *The Astrophysical Journal Letters* **2021**, *918*, L28.
17. Riley, T.E.; Watts, A.L.; Ray, P.S.; Bogdanov, S.; Guillot, S.; Morsink, S.M.; Bilous, A.V.; Arzoumanian, Z.; Choudhury, D.; Deneva, J.S.; et al. A NICER view of the massive pulsar PSR J0740+ 6620 informed by radio timing and XMM-Newton spectroscopy. *The Astrophysical Journal Letters* **2021**, *918*, L27.
18. Doroshenko, V.; Suleimanov, V.; Pühlhofer, G.; Santangelo, A. A strangely light neutron star within a supernova remnant. *Nature Astronomy* **2022**, *6*, 1444–1451.
19. Kini, Y.; Salmi, T.; Vinciguerra, S.; Watts, A.L.; Bilous, A.; Galloway, D.K.; van der Wateren, E.; Khalsa, G.P.; Bogdanov, S.; Buchner, J.; et al. Constraining the properties of the thermonuclear burst oscillation source XTE J1814- 338 through pulse profile modelling. *Monthly Notices of the Royal Astronomical Society* **2024**, *535*, 1507–1525.
20. Weber, F. Strange quark matter and compact stars. *Progress in Particle and Nuclear Physics* **2005**, *54*, 193–288.
21. Witten, E. Cosmic separation of phases. *Physical Review D* **1984**, *30*, 272.
22. Itoh, N. Hydrostatic equilibrium of hypothetical quark stars. *Progress of Theoretical Physics* **1970**, *44*, 291–292.
23. Farhi, E.; Jaffe, R.L. Strange matter. *Physical Review D* **1984**, *30*, 2379.
24. Ivanenko, D.; Kurdgelaidze, D. Hypothesis concerning quark stars. *Astrophysics* **1965**, *1*, 251–252.
25. Drake, J.J.; Marshall, H.L.; Dreizler, S.; Freeman, P.E.; Fruscione, A.; Juda, M.; Kashyap, V.; Nicastro, F.; Pease, D.O.; Wargelin, B.J.; et al. Is RX J1856. 5–3754 a quark star? *The Astrophysical Journal* **2002**, *572*, 996.
26. Bombaci, I. Observational evidence for strange matter in compact objects from the x-ray burster 4U 1820-30. *Physical Review C* **1997**, *55*, 1587.
27. Lattimer, J.M. The nuclear equation of state and neutron star masses. *Annual Review of Nuclear and Particle Science* **2012**, *62*, 485–515.
28. Dai, Z.G.; Wang, S.Q.; Wang, J.; Wang, L.J.; Yu, Y.W. The most luminous supernova ASASSN-15LH: signature of a newborn rapidly rotating strange quark star. *The Astrophysical Journal* **2016**, *817*, 132.
29. Chodos, A.; Jaffe, R.L.; Johnson, K.; Thorn, C.B.; Weisskopf, V. New extended model of hadrons. *Physical Review D* **1974**, *9*, 3471.
30. Chodos, A.; Jaffe, R.; Johnson, K.; Thorn, C.B. Baryon structure in the bag theory. *Physical Review D* **1974**, *10*, 2599.
31. Alford, M.; Rajagopal, K.; Wilczek, F. QCD at finite baryon density: Nucleon droplets and color superconductivity. *Physics Letters B* **1998**, *422*, 247–256.
32. Nambu, Y.; Jona-Lasinio, G. Dynamical model of elementary particles based on an analogy with superconductivity. II. *Physical review* **1961**, *124*, 246.
33. Szabó, K.K.; Tóth, A.I. Quasiparticle description of the QCD plasma, comparison withlattice results at finite T and μ. *Journal of High Energy Physics* **2003**, *2003*, 008.
34. Peng, G.; Chiang, H.; Yang, J.; Li, L.; Liu, B. Mass formulas and thermodynamic treatment in the mass-density-dependent model of strange quark matter. *Physical Review C* **1999**, *61*, 015201.
35. Dyson, F.J. The S matrix in quantum electrodynamics. *Physical Review* **1949**, *75*, 1736.
36. Schwinger, J. On the Green's functions of quantized fields. II. *Proceedings of the National Academy of Sciences* **1951**, *37*, 455–459.
37. Chen H, Yuan W, L.Y.X. Partial restoration of chiral symmetry versus quark number density at zero temperature. *Journal of Physics G: Nuclear and Particle Physics* **2009**, *36*, 064073.
38. Chen, H.; Baldo, M.; Burgio, G.; Schulze, H.J. Hybrid stars with the Dyson-Schwinger quark model. *Physical Review D* **2011**, *84*, 105023.
39. Klähn, T.; Roberts, C.D.; Chang, L.; Chen, H.; Liu, Y.X. Cold quarks in medium: An equation of state. *Physical Review C—Nuclear Physics* **2010**, *82*, 035801.
40. Zwicky, F. Die rotverschiebung von extragalaktischen nebeln. *Helvetica Physica Acta* **1933**, *6*, 110–127.
41. Rubin, V.C.; Ford Jr, W.K. Rotation of the Andromeda nebula from a spectroscopic survey of emission regions. *Astrophysical Journal* **1970**, *159*, 379.

 doi:10.20944/preprints202602.1818.v1

42. Clowe, D.; Bradač, M.; Gonzalez, A.H.; Markevitch, M.; Randall, S.W.; Jones, C.; Zaritsky, D. A direct empirical proof of the existence of dark matter. *The Astrophysical Journal* **2006**, *648*, L109.
43. Ade, P.A.; Aghanim, N.; Arnaud, M.; Ashdown, M.; Aumont, J.; Baccigalupi, C.; Banday, A.; Barreiro, R.; Bartlett, J.; Bartolo, N.; et al. Planck 2015 results-xiii. cosmological parameters. *Astronomy & Astrophysics* **2016**, *594*, A13.
44. Baryakhtar, M.; Caputo, R.; Croon, D.; et al. Dark Matter In Extreme Astrophysical Environments. *arXiv preprint arXiv:2203.07984* **2022**.
45. Billard, J.; Boulay, M.; Cebrián, S.; Covi, L.; Fiorillo, G.; Green, A.; Kopp, J.; Majorovits, B.; Palladino, K.; Petricca, F.; et al. Direct detection of dark matter—APPEC committee report. *Reports on Progress in Physics* **2022**, *85*, 056201.
46. Goldman, I.; Nussinov, S. Weakly interacting massive particles and neutron stars. *Physical Review D* **1989**, *40*, 3221.
47. Kouvaris, C. WIMP annihilation and cooling of neutron stars. *Physical Review D* **2008**, *77*, 023006.
48. Kaplan, D.E.; Luty, M.A.; Zurek, K.M. Asymmetric dark matter. *Physical Review D* **2009**, *79*, 115016.
49. Kouvaris, C.; Tinyakov, P. Constraining Asymmetric Dark Matter through observations of compact stars. *Physical Review D* **2011**, *83*, 083512.
50. Kain, B. Radial oscillations and stability of multiple-fluid compact stars. *Physical Review D* **2020**, *102*, 023001.
51. Das, H.; Kumar, A.; Kumar, B.; Patra, S.K. Dark matter effects on the compact star properties. *Galaxies* **2022**, *10*, 14.
52. Hippert, M.; Dillingham, E.; Tan, H.; Curtin, D.; Noronha-Hostler, J.; Yunes, N. Dark matter or regular matter in neutron stars? How to tell the difference from the coalescence of compact objects. *Physical Review D* **2023**, *107*, 115028.
53. Routaray, P.; Das, H.; Sen, S.; Kumar, B.; Panotopoulos, G.; Zhao, T. Radial oscillations of dark matter admixed neutron stars. *Physical Review D* **2023**, *107*, 103039.
54. Bramante, J.; Raj, N. Dark matter in compact stars. *Physics Reports* **2024**, *1052*, 1–48.
55. Sotani, H.; Kumar, A. Emergence of new oscillation modes in dark matter admixed neutron stars. *Physical Review D* **2025**, *111*, 123013.
56. Mukhopadhyay, P.; Schaffner-Bielich, J. Quark stars admixed with dark matter. *Physical Review D* **2016**, *93*, 083009.
57. Panotopoulos, G.; Lopes, I. Radial oscillations of strange quark stars admixed with condensed dark matter. *Physical Review D* **2017**, *96*, 083013.
58. Panotopoulos, G.; Lopes, I. Radial oscillations of strange quark stars admixed with fermionic dark matter. *Physical Review D* **2018**, *98*, 083001.
59. Lopes, L.L.; Das, H. Strange stars within bosonic and fermionic admixed dark matter. *Journal of Cosmology and Astroparticle Physics* **2023**, *2023*, 034.
60. Yang, Y.; Wu, C.; Yang, J.F. Impact of dark matter on strange quark stars described by different quark models. *The European Physical Journal C* **2025**, *85*, 426.
61. Jiménez, J.C.; Fraga, E.S. Radial oscillations of quark stars admixed with dark matter. *Universe* **2022**, *8*, 34.
62. Zhen, Y.; Sun, T.T.; Wei, J.B.; Zheng, Z.Y.; Chen, H. Radial Oscillations of Strange Quark Stars Admixed with Dark Matter. *Symmetry* **2024**, *16*, 807.
63. Yang, S.H.; Pi, C.M. Color-flavor locked strange stars admixed with mirror dark matter and the observations of compact stars. *Journal of Cosmology and Astroparticle Physics* **2024**, *2024*, 052.
64. Yang, S.H.; Pi, C.M.; Weber, F. Strange stars admixed with mirror dark matter: Confronting observations of XTE J1814-338. *Physical Review D* **2025**, *111*, 043037.
65. Panotopoulos, G.; Rincón, Á.; Lopes, I. Exploring the structural properties of anisotropic dark matter-admixed quark stars. *Physics of the Dark Universe* **2025**, p. 101972.
66. Lugones, G.; Horvath, J.E. Color-flavor locked strange matter. *Physical Review D* **2002**, *66*, 074017.
67. Flores, C.V.; Lugones, G. Constraining color flavor locked strange stars in the gravitational wave era. *Physical Review C* **2017**, *95*, 025808.
68. Chavanis, P.H.; Harko, T. Bose-Einstein condensate general relativistic stars. *Physical Review D* **2012**, *86*, 064011.
69. Ciarcelluti, P.; Sandin, F. Have neutron stars a dark matter core? *Physics Letters B* **2011**, *695*, 19–21.
70. Damour, T.; Nagar, A. Relativistic tidal properties of neutron stars. *Physical Review D* **2009**, *80*, 084035.
71. Takátsy, J.; Kovács, P. Comment on "Tidal Love numbers of neutron and self-bound quark stars". *Physical Review D* **2020**, *102*, 028501.

 doi:10.20944/preprints202602.1818.v1

72. Hinderer, T. Tidal Love numbers of neutron stars. *The Astrophysical Journal* **2008**, *677*, 1216.
73. Cronin, J.; Zhang, X.; Kain, B. Rotating dark matter admixed neutron stars. *Physical Review D* **2023**, *108*, 103016.
74. Postnikov, S.; Prakash, M.; Lattimer, J.M. Tidal Love numbers of neutron and self-bound quark stars. *Physical Review D* **2010**, *82*, 024016.
75. Abbott, R.; Abbott, T.; Abraham, S.; Acernese, F.; Ackley, K.; Adams, C.; Adhikari, R.X.; Adya, V.; Affeldt, C.; Agathos, M.; et al. GW190814: gravitational waves from the coalescence of a 23 solar mass black hole with a 2.6 solar mass compact object. *The Astrophysical Journal Letters* **2020**, *896*, L44.
76. Romani, R.W.; Kandel, D.; Filippenko, A.V.; Brink, T.G.; Zheng, W. PSR J0952- 0607: The fastest and heaviest known galactic neutron star. *The Astrophysical Journal Letters* **2022**, *934*, L17.
77. Leung, S.C.; Chu, M.C.; Lin, L.M. Dark-matter admixed neutron stars. *Physical Review D* **2011**, *84*, 107301.